Multiple Wavefront Shaping by Metasurface Based on Mixed Random Antenna Groups
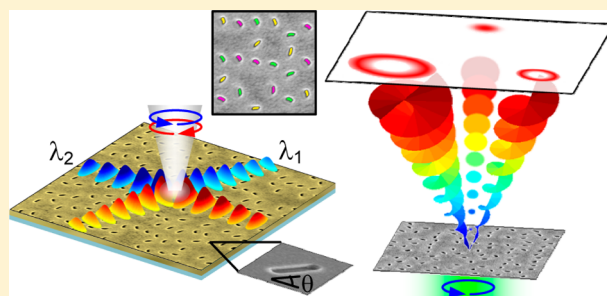
Dekel Veksler, Elhanan Maguid, Nir Shitrit, Dror Ozeri, Vladimir Kleiner, and Erez Hasman*

Micro and Nanooptics Laboratory, Faculty of Mechanical Engineering, and Russell Berrie Nanotechnology Institute, Technion—Israel Institute of Technology, Haifa 32000, Israel

ⓢ Supporting Information

ABSTRACT: Photonic gradient metasurfaces are ultrathin electromagnetic wave-molding metamaterials that provide a route for realizing flat optics. However, the up-to-date metasurface design, manifested by imprinting the required phase profile for a single, on-demand light manipulation functionality, is not compatible with the desired goal of multifunctional flat optics. Here, we report on a generic concept to control multifunctional optics by disordered (random) gradient metasurfaces with a custom-tailored geometric phase. This approach combines the peculiar ability of random patterns to support an extraordinary information capacity and the polarization helicity control in the geometric phase mechanism, simply implemented in a two-dimensional structured matter by imprinting optical antenna patterns. By manipulating the local orientations of the nanoantennas, we generate multiple wavefronts with different functionalities via mixed random antenna groups, where each group controls a different phase function. Disordered gradient metasurfaces broaden the applicability of flat optics, as they offer all-optical manipulation by multitask wavefront shaping via a single ultrathin nanoscale photonic device.

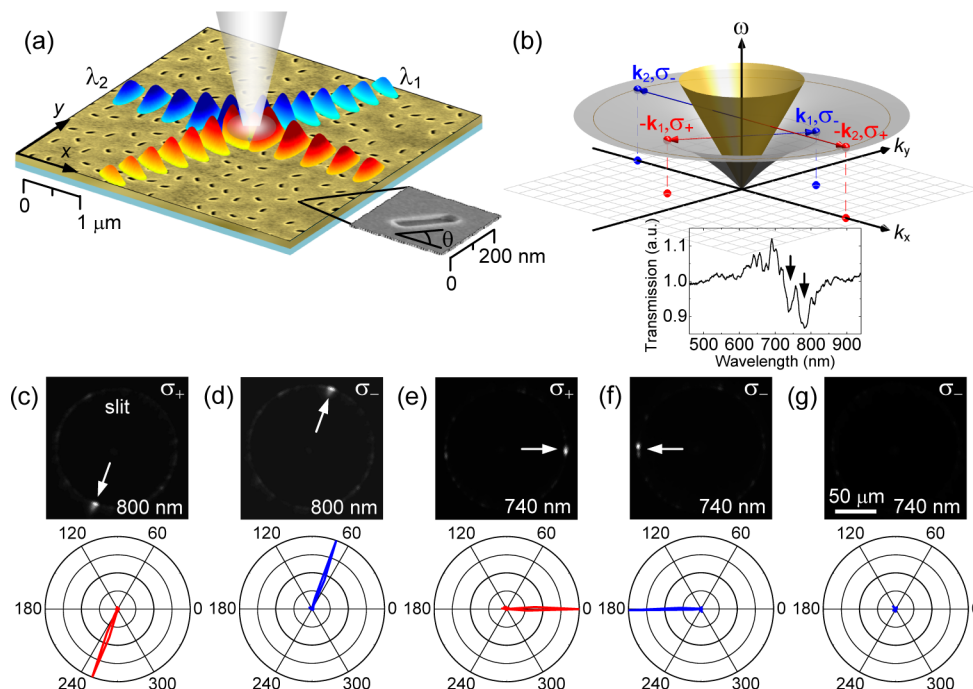**KEYWORDS:** metasurfaces, disorder, geometric phase, multifunctional optics, polarization, angular momentum

The ability to control the flow of light beyond that offered by conventional optics has significantly improved owing to the rapidly expanding field of photonic metasurfaces.[1−4] Photonic metasurfaces, i.e., metamaterials with a reduced dimensionality composed of engineered subwavelength-scale meta-atoms, pave the way for realizing flat optics by replacing bulky optical components with ultrathin planar elements.[3,4] Moreover, two-dimensional metasurfaces are of particular interest, as they may serve as the missing link for the integration of nanophotonic chips with nanoelectronic circuits. An extra twist in this field originates from gradient metasurfaces enabling light manipulation by inducing on the incident electromagnetic wave local transversely nonuniform abrupt changes of the phases over a subwavelength distance.[1,2,5−7] By molding the polarization[8] and linear or angular momenta,[5,9,10] custom-tailored gradient metasurfaces have been created to serve as ultrathin planar optical devices.[3,4,7,11,12] Gradient metasurfaces are realized in either dielectric−dielectric[2,7,11] or metal−dielectric interfaces,[5,6,8−10,12,13] where in the latter propagating surface-confined waves of surface plasmon polaritons (SPPs, resonant collective oscillations of quasi-free electrons at the metal surface[14]) mediate the in- and out-coupling of light. The approaches for obtaining gradient metasurfaces with a desired space-variant phase are scaling the dimensions of isotropic[15] or anisotropic phase-imprinted meta-atoms in a nonuniform manner[5,13,16] or nonuniformly orientating the local angle of anisotropic meta-atoms;[9,10] the
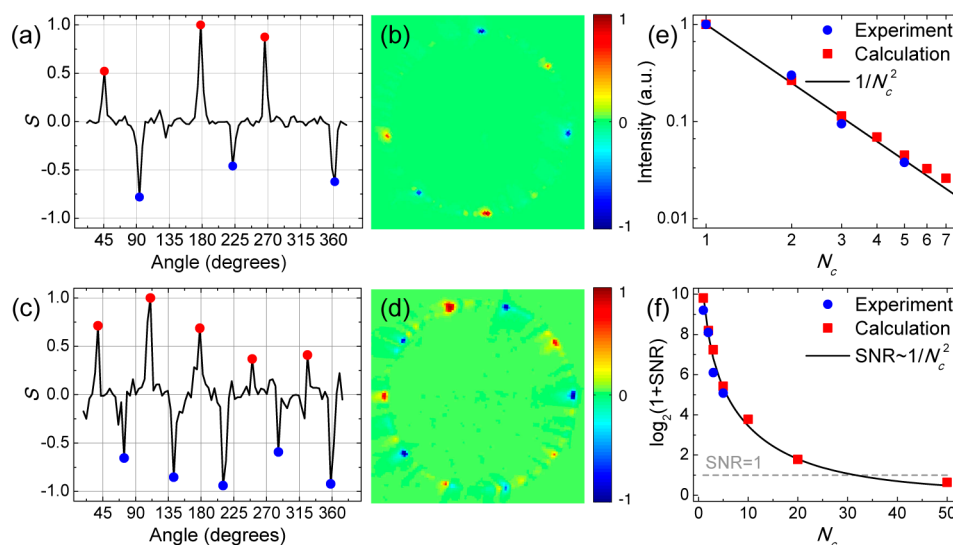
first concept requires the design and fabrication of different meta-atoms according to the phase increment, whereas in the second concept, utilizing the Pancharatnam−Berry phase, the same meta-atoms are used.

The Pancharatnam−Berry phase[17] is a promising approach for achieving an abrupt phase change leveraging the design of gradient metasurfaces, as originally presented in ultrathin metallic[1] and dielectric phase optical elements.[2] The peculiarity of this phase lies in its geometric nature; unlike diffractive and refractive elements, it does not arise from optical path differences but from a space-variant manipulation of the light polarization state.[1,2,7,9−11] When an incident circularly polarized light is scattered from a metasurface consisting of subwavelength anisotropic antennas whose local orientation angle is $\theta(x, y)$, a geometric phase shift of $\phi_g(x, y) = 2\sigma\theta$ is induced, where $\sigma_{\pm} = \pm 1$ is the photon spin corresponding to right and left circular polarizations, respectively.[2,9,10] Apparently, the optical spin provides an additional degree of freedom in nano-optics for spin degeneracy removal phenomena in gradient metasurfaces,[6,7,9,10] such as polarization-controlled directional excitation of SPPs.[18−21] The presented unidirectional launching[18−20] via periodic gradient metasurfaces suffers from the limitation of a single channel; moreover, the observed multidirectional excitation[21] reveals the constraints of a
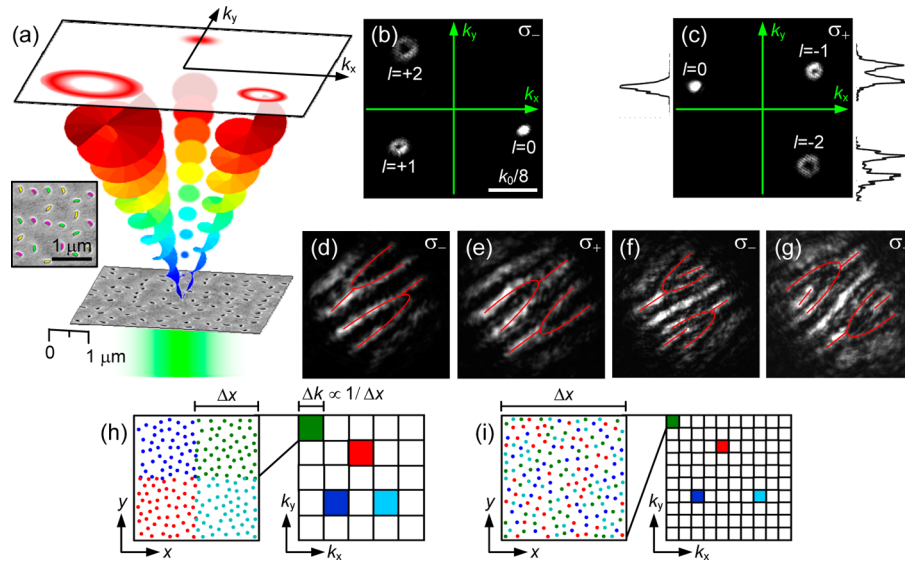
Figure 1. Near-field open channels via disordered gradient metasurfaces. (a) Schematic of directional SPP channels opened by a DGM. The scanning electron microscope image shows the $10 \times 10\ \mu m^2$ metasurface, wherein $r_{min} = 300$ nm and $d \approx 520$ nm, fabricated using a focused ion beam. The array consists of 80-by-220 nm^2 nanoantennas, etched to a depth of 100 nm into a 200 nm thick gold film, evaporated onto a glass substrate. The diameter and width of the surrounding annular slit (not shown) are 150 μm and 150 nm, respectively. (b) Dispersion relation of free-space light (conic manifold) and SPPs (curved manifold). Red and blue arrows correspond to directional SPP coupling by normally incident light with $\sigma_{\pm}$ spin states, respectively. The inset shows the measured transmission spectrum of the two-channel metasurface (with aperture nanoantennas), normalized to the transmission spectrum of a randomly oriented nanoantenna metasurface. (c, d) Measured intensities of open channels and corresponding azimuthal cross sections along the slit for $\sigma_{\pm}$ illuminations, respectively, at a wavelength of 800 nm. In the polar representation, the azimuthal angle is given in degrees and the intensity is on a linear scale. (e, f) Measured intensities and azimuthal cross sections for $\sigma_{\pm}$, respectively, at a wavelength of 740 nm. (g) Measured behavior of a metasurface with randomly oriented nanoantennas.

Figure 2. Information capacity analysis of a near-field multichannel disordered gradient metasurface. (a−d) Spin-controlled open channels with different numbers of multiple channels at a wavelength of 740 nm. The measurements of $S = (I_{\sigma_+} - I_{\sigma_-})/\max(I_{\sigma_+} - I_{\sigma_-})$, where $I_{\sigma_\pm}$ is the intensity for $\sigma_{\pm}$ excitations, respectively, along the slit show the 3×2 (panels a and b) and 5×2 (panels c and d) open channels from different metasurfaces. This measurement procedure was performed to reduce the experimental setup noise. Red and blue spots in panels b and d correspond to open channels for incident $\sigma_{\pm}$ spin states, respectively. (e) Dependence of the signal intensity on number of open channels. (f) Number of bits per channel for varying number of open channels. The calculation was performed with a constant total number of antennas.

directional dependence between channels arising from the lattice symmetry and limited number of channels due to rotational symmetry restrictions of a periodic gradient metasur-

face crystal. These disadvantages impose limitations on the growing demand of multiple wavefronts with independent directions and wavelengths for multifunctional metasurface

Figure 3. Free-space multiple wavefront shaping based on a disordered gradient metasurface. (a) Schematic of spin-controlled far-field phase functions with different orbital angular momenta generated by a DGM. The inset shows the mixed antenna groups, where each color corresponds to a different wavefront. (b, c) Measured spin-flip momentum deviations of three wavefronts with different orbital angular momenta for σ_- and σ_+ spin states of the scattered light, respectively, at a wavelength of 740 nm. The intensity cross sections of the different orbital AM orders, presented at the side of the image, visualize the different dislocation strengths. The polarization state is resolved with the use of a circular polarization analyzer (a quarter-wave plate followed by a linear polarizer). (d−g) Measured interference patterns of the spin-flip components generated by two identical overlapped orbital AM orders. The patterns were observed from different DGMs forming wavefronts with $l = \pm1$ (panels d and e) and $l = \pm2$ (panels f and g) for σ_- and σ_+ scattered spin states, respectively. Note that this method enables the simultaneous measurement of the strength and the helicity of the dislocation. (h, i) Metasurfaces divided into separated and mixed channel regions, respectively. The reciprocal spaces show that the channel capacity in the mixed channel type is significantly higher.

devices. We offer an approach to overcome the limitations of polarization-controlled directional excitation, thus expanding its scope via disordered gradient metasurfaces (DGMs) with a custom-tailored geometric phase.

Previous research in the field of metasurfaces focused on ordered structures. Disordered systems were rarely addressed, despite increasing scientific interest in the field of disordered photonics.[22−24] The exploration of new phenomena in random metasurfaces via coherent effects associated with disordered bulk media, such as backscattering,[25] enhanced transmission via coupling to eigenmodes,[26,27] and focusing through scattering media,[28,29] has inspired even greater interest. Recently, phenomena related to random metasurfaces have been under investigation; among them are broadband and wide angle absorbers for solar cells,[30] localized electromagnetic fields,[31,32] and second-harmonic generation.[33] Here, we report on a novel generic concept for multifunctional photonics with independent phase and amplitude control exploiting the peculiarities of DGMs. By utilizing the geometric phase, induced by the degree of freedom of an anisotropic nanoantenna orientation, we fulfill a hybrid location−orientation phase-matching condition that enables opening multiple on-demand spin-dependent channels (i.e., directional constructive interferences) in passive gradient metasurfaces with randomly distributed antennas in both near (see Figure 1a) and far fields (see Figure 3a). The multichannel DGM is composed of mixed random antenna groups with different functionalities, where each group independently controls a different wavefront. We revealed extraordinary channel capacity within the intrinsic limit of speckle noise in DGMs and observed state-of-the-art spin-controlled multiple wavefront shaping and structured-light interconnects. Spin-optical DGMs may facilitate the replacement of complex optical systems by an individual multifunctional metasurface device.

In addition to the spin angular momentum (AM) of $\sigma_\pm\hbar$ per photon associated with the circular polarization handedness, a light field can also carry an orbital AM of $l\hbar$ per photon associated with its spiral phase front $e^{-il\varphi}$, where the integer number l is the topological charge and φ is the azimuthal angle.[34] The scattering from an isotropic nanohole, excited by circularly polarized light, results in a propagating SPP wave acquiring an orbital AM that is equal to the incident spin AM.[35] The arising spin-based plasmonic electric field in polar coordinates (r, φ) is $E(\sigma) \propto e^{i(kr-\sigma\varphi)}/\sqrt{r}$, where σ is the incident optical spin, $k(\omega)$ is the SPP wavenumber, and ω is the frequency of light. The AM conservation in this light−matter interaction originates from the circular symmetry of the scatterer. However, when an anisotropic nanoantenna is considered as a source, the AM is not conserved and an additional wave with an opposite orbital AM is generated (see Supporting Information Section 1 for a detailed analysis), so

$$E(\sigma) \propto \left(e^{i(kr-\sigma\varphi)} + e^{i(kr+\sigma\varphi-2\sigma\theta)}\right)/\sqrt{r} \qquad (1)$$

Note that the secondary surface wave is accompanied by a geometric phase of $-2\sigma\theta$ (Supporting Information Section 1). By considering a metasurface consisting of an ensemble of uncoupled nanoantennas, the global SPP field is the coherent superposition of all the elemental fields. At an observation point far from the ensemble, the emerged field is

$$E(\mathbf{k}, \sigma) \propto e^{-i\sigma\overline{\varphi}} \sum_{n}^{N} e^{-i\mathbf{k}\cdot\mathbf{r}_n} + e^{i\sigma\overline{\varphi}} \sum_{n}^{N} e^{-i(\mathbf{k}\cdot\mathbf{r}_n+2\sigma\theta_n)}$$

where $\overline{\varphi}$ is the mean azimuthal angle of observation, N is the total number of antennas per channel, and $\mathbf{r}_n$ and θ_n are the position vector and the orientation of the nth antenna, respectively.

The scattered field component $\sum_n^N e^{-i(\mathbf{k}\cdot\mathbf{r}_n + 2\sigma\theta_n)}$ can be regarded as the structure factor of a metasurface, whereas the geometric phase is the spin-dependent atomic form factor of a nanoantenna.[36] Although a random distribution of the nanoantenna locations is considered, a proper selection of the antenna orientations results in a constructive interference when the phase-matching condition $\mathbf{k}\cdot\mathbf{r}_n + 2\sigma\theta_n = 2\pi m$ is fulfilled for an arbitrary integer m. We regard anisotropic antennas of nanorods whose local orientation is mod π defined; hence, the above condition is reduced to

$$2\theta_n = \mathbf{k}_g\cdot\mathbf{r}_n \tag{2}$$

where $\mathbf{k}_c = -\sigma\mathbf{k}_g$ is the desired channel wave vector. Accordingly, a spin-controlled channel is opened in a predetermined direction of $\mp\hat{\mathbf{k}}_c$ for $\sigma_\pm$ excitations, respectively. The sums in the scattered field $\sum_n^N e^{-i\mathbf{k}\cdot\mathbf{r}_n}$ and $\sum_n^N e^{-i(\mathbf{k}-\mathbf{k}_c)\cdot\mathbf{r}_n}$ can be evaluated by Monte Carlo integration theory.[37] This results in a zero (ballistic) diffraction order and the desired open channel, respectively, accompanied by a speckle noise $\varepsilon(\mathbf{k}) \propto O(\sqrt{N})$, i.e., a random distribution resulting from the coherent interference of wavefronts scattered from a fine-scale granular pattern.[38] Consequently, the total scattered field arises in a spin-dependent open channel expressed as $E(\mathbf{k}, \sigma) \propto N\Delta((\mathbf{k} + \sigma\mathbf{k}_g)D) + \varepsilon(\mathbf{k})$, where $\Delta(\mathbf{p}) \equiv \mathrm{sinc}(p_x)\,\mathrm{sinc}(p_y)$, and D is the metasurface width.

The introduced concept enables the design of multiple directional channels by a random mixing of antennas with different orientation functions in a single metasurface, where each channel is individually controlled by the wavelength and the polarization helicity of the incident light (see Figure 1b). The number of open channels N_c is restricted by the characteristic distance between antennas in each channel, $d \approx (A/N)^{1/2}$, and the minimal separation between neighboring antennas of $r_{\min} \approx (A/N_t)^{1/2}$, determined by fabrication limitations and the requirement for eliminating the coupling between nanoantennas.[35] Here, A is the metasurface area and $N_t = NN_c$ is the total number of antennas. Accordingly, the geometric limit for the metasurface channel capacity is $N_c^{(g)} \approx (d/r_{\min})^2$. For a random distribution of the antenna positions, there is no restriction on the distance d for opening a single channel. On the other hand, for an ordered (periodic) antenna distribution, the scattered field consists of diffraction orders as manifested by the momentum-matching condition $\mathbf{k}_c = -\sigma\mathbf{k}_g + i\mathbf{G}_1 + j\mathbf{G}_2$, where $(\mathbf{G}_1, \mathbf{G}_2) = 2\pi/d(\hat{\mathbf{x}}, \hat{\mathbf{y}})$ are the reciprocal lattice vectors. Here, a single channel ($i = j = 0$) is obtained only for a subwavelength structure with $d < \lambda_c/2$, where $\lambda_c = 2\pi/k_c$. This implies that DGMs provide an enormous advantage compared to ordered systems, as they enable a sampling of the desired phase profile with $d \gg \lambda_c/2$, which is essential for opening multiple channels under the geometric limitation of $N_c^{(g)}$ (Supporting Information Section 2).
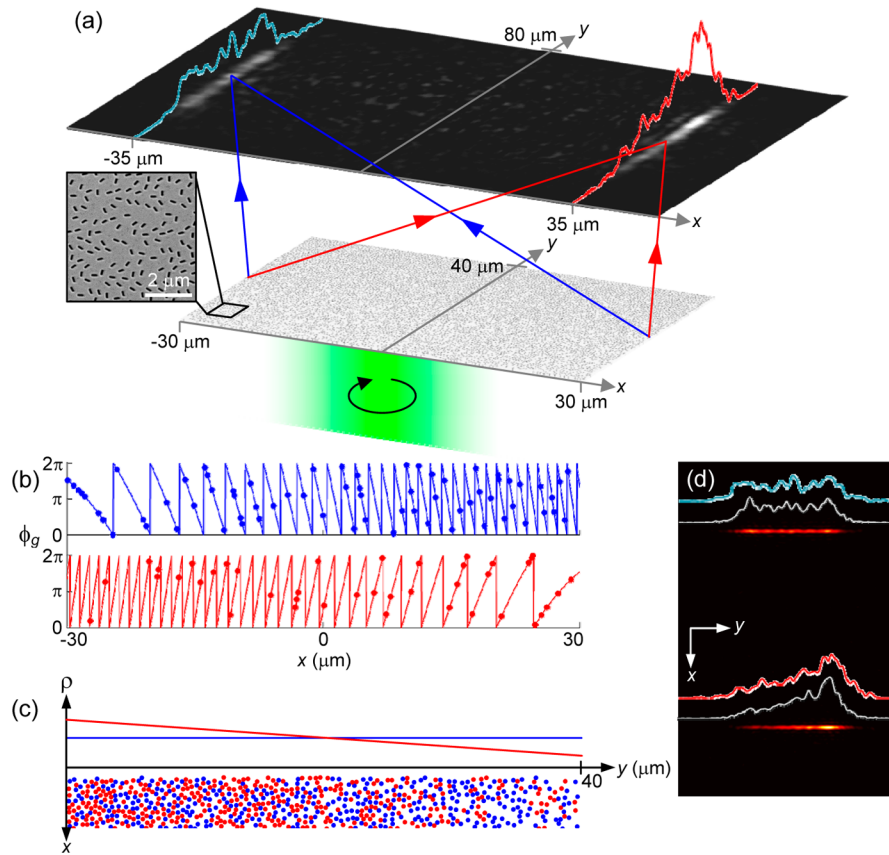
Plasmonic DGMs were realized for the experimental observation of open channels in the near field. For each chosen channel, we control the propagation direction of the SPPs, which are launched by an array consisting of anisotropic void nanoantennas at random locations, by tuning the local antenna orientation (eq 2). We implemented two spin-dependent channels operating at different incident wavelengths. Accordingly, the total number of antennas was randomly divided into two equal mixed groups. The first antenna group opened a spin-based SPP channel at the wavelength of 740 nm in 0° and 180° directions for $\sigma_\pm$ (Figure 1e,f), respectively, whereas the second group opened a channel at 800 nm in 250°

and 70° for $\sigma_\pm$, respectively (Figure 1c,d). The fabricated metasurface was surrounded by an annular decoupling slit enabling free-space imaging of SPP jets launched from the antenna array. The metasurface was normally illuminated with a continuous wave Ti-sapphire tunable laser via a circular polarizer. The spin-controlled multichannel excitation was observed by measuring the intensity distributions along the slit (Figure 1c−f). These spin-based open channels via a DGM were verified by calculated SPP intensity distributions (see Supporting Information Section 3), obtained by the superposition of scattered fields from anisotropic antennas with designed orientations (eq 1). Note that when the antenna orientations are randomly set, open channels are not observed (Figure 1g). The light-to-SPPs coupling efficiency of a DGM with a single near-field channel was found to be ∼15% via a numerical evaluation (see Supporting Information Section 4).

We also measured the transmission spectrum of the metasurface with mixed antenna groups, and the signature of the operating wavelengths of the open channels is observed as antiresonances in the corresponding SPP wavelengths (Figure 1b, inset; see also Supporting Information Section 5). We further increased the number of open channels in the near field to observe 3 × 2 azimuthally nonequidistant (Figure 2a,b) and 5 × 2 equidistant spin-dependent channels (Figure 2c,d) in predetermined directions. Note that the obtained asymmetric excitation pattern in Figure 2a,b cannot be generated by a lattice, and the 10-fold symmetric pattern in Figure 2c,d can be generated only by a quasicrystal; hence, these demonstrations manifest the all-optical manipulation by DGMs.

Several critical issues arise when characterizing the near-field information capacity of a multichannel DGM: diffraction, noise, crosstalk, and geometry. From a diffraction limit consideration, the upper limit for the number of channels is $N_c^{(d)} \approx 2\pi D/\lambda_{SPP}$, where λ_{SPP} is the SPP wavelength. In addition, the origin of the system noise is a speckle pattern and the crosstalk between channels. The signal-to-noise ratio (SNR), which determines the number of bits per channel of $\log_2(1 + \mathrm{SNR})$, provides a limit for the channel capacity of $N_c^{(n)}$, set by $\mathrm{SNR} \approx 1$. The measured open channels from a DGM show that the crosstalk between the multiple channels is rather weak (see Supporting Information Section 6). Regarding the dependence of the signal intensity in the open channel number, we investigated a series of gradient metasurfaces with a single and multiple spin-controlled channels by measuring the average intensity of channels (Figure 2e). The observed experimental trend coincides with a calculation based on the interference model (Supporting Information Section 7) showing that the intensity of each channel scales as $(N_t/N_c)^2$ (Figure 2e), as originally introduced in multiplex holograms.[39] Moreover, the calculation reveals that the noise intensity scales as N_t, so the SNR is proportional to N_t/N_c^2 (Figure 2f), as experimentally observed in the single- and multiple-channel metasurfaces. For a chosen gradient metasurface with a relatively small area of 10 × 10 μm^2, we obtain a channel capacity upper limit of $N_c^{(d)} \approx 90$, whereas the actual limitation of $N_c^{(n)} \approx 30$ (Figure 2f), offering a multichannel design of tens of open channels.

DGMs can also generate multiple phase functions in the far field, providing the route for free-space interconnects. Optical interconnects offer low crosstalk, high bandwidth, and parallel operation, making them attractive for analog and digital optical computing as well as for electronic chips.[40] DGMs may serve as a promising platform for state-of-the-art optical interconnects manifested by controlling the transverse phase distribution in

Figure 4. Phase and amplitude control by a disordered gradient metasurface. (a) Schematic of two deflected spin-dependent cylindrical lenses with uniform and gradient focal line intensity distributions generated by a single DGM. The imprinted geometric phase profiles are $\phi_g = 2\sigma\pi(((x \mp 35)^2 + f^2)^{1/2} - f)/\lambda$ for the channels with a gradient and a uniform d, respectively, where $f = 72$ μm is the focal length of the lens. Note that for σ_+ the metasurface operates as a focusing lens, whereas for σ_- it operates as a diverging lens. (b) Geometric phase profiles and nanoantenna distributions of the two cylindrical lenses imprinted in the DGM. Blue (top) and red (bottom) dots represent the locations of the nanoantennas in the lenses with a uniform and a gradient d, respectively. The locations in the phase profiles were obtained from a wavelength-width strip. (c) Profile of the density of antennas for the mixed antenna groups in the two-channel DGM. The characteristic distances of the uniform and gradient channels are $d \approx 700$ nm and $d \approx 0.5-1$ μm, respectively. (d) Measured and calculated intensity distributions along the focal lines of the lenses with a uniform (top) and a gradient (bottom) d, at a wavelength of 800 nm. The white lines represent the calculated intensity obtained by the Huygens principle with a geometric phase delay ($E = \sum e^{i(\mathbf{k}\cdot\mathbf{r} + 2\sigma\theta(x,y))}/r$).

addition to the propagation direction (see Supporting Information Section 8 for multiple far-field wavefronts of plane waves). The generation of free-space nonuniform wavefronts, such as helical phase fronts, results in interconnects based on the orbital AM. We demonstrated a general fan-out structured-light shaping based on an ultrathin spin-optical DGM (Figure 3a). By orientating the nanoantennas of each wavefront according to $2\theta(x, y) = \alpha x + l\varphi$, a spin-controlled free-space wavefront with an independent design of the propagation direction and the orbital AM is generated. The corresponding scattered component carries an orbital AM of σl and undergoes deflection at an angle of $\arcsin(\sigma\alpha/k_0)$, where k_0 and σ are the wavenumber and the spin state of the incident beam, respectively; moreover, the scattered component is manifested by a spin flip to an opposite spin state with regard to the incident beam.[2,7,9,10] We observed 3×2 spin-dependent wavefronts in desired directions with different orbital angular momenta (Figure 3b,c), where the strength and the helicity of the dislocation were verified by interference patterns of vortex beams (Figure 3d−g). The peculiar property of the disordered approach that enables generation of multiple wavefronts with $d > \lambda/2$ was also presented via a metasurface wherein $d \approx 2\lambda$ (see Supporting Information Section 8). Note that the generation of

far-field phase functions does not require a matching to the SPP momentum, thereby making their operation independent of wavelength (see Supporting Information Section 9) within the broad polarization-based spectral response of the anisotropic antenna (see Supporting Information Section 10). The introduced ability to utilize light control by DGMs for interconnects paves the way for controlling general light transport via spin-optical DGMs with mixed groups of nanoantennas, where each group has a different beam-shaping task.

The channel capacity of free-space optical interconnects based on metasurfaces with mixed antenna groups can be analyzed by the Gabor theory of information.[41] Multiple channels can be opened by two types of metasurfaces wherein the area is divided into N_c separated regions (Figure 3h), or the nanoantennas of each channel are randomly distributed over the entire area (Figure 3i). For a given solid angle of Ω, the diffraction limit of each channel (assuming plane waves) states that for the first type $N_c \approx (A\Omega/\lambda^2)^{1/2}$, whereas for the mixed channel type, according to the Gabor limit, $N_c \approx (A\Omega/\lambda^2)$.[41,42] Consequently, the information capacity of the presented DGM is significantly higher than the separated channel regions (see Figure 3h,i).

Beyond imprinting any desired phase distribution, DGMs also offer an additional advantage of local amplitude control. By locally changing the channel characteristic distance $d(x, y)$, we control the local density of antennas ρ and thus the space-variant wavefront amplitude $E_c(x, y) \propto \sqrt{\rho} = 1/d$. We demonstrated the amplitude control by realizing two cylindrical focusing lenses in a single DGM, where the first antenna group opens a channel with a uniform d and the second antenna group opens a channel with a space-variant d (Figure 4a−c). The observed focal line from the nonuniform cylindrical lens shows a gradient intensity profile (Figure 4d, bottom) with respect to the reference measurement of the uniform cylindrical lens showing a uniform intensity (Figure 4d, top). Hence, DGMs with an electromagnetic field of $E_c(d(x, y))e^{i2\sigma\theta(x,y)}$ enable independent amplitude and phase control via the space-variant channel characteristic distance and the local antenna orientation, respectively.

The reported proof-of-concept of multiple wavefront shaping in the far field showed a low efficiency due to the weak coupling between the incident wave and void nanoantenna modes. This efficiency can be dramatically increased by properly designing the birefringent phase retardation of the metasurface nanoscale unit cell, as presented in dielectric[7] and gap plasmon-based gradient metasurfaces,[16] thus leveraging the introduced principle to provide high-efficiency metasurface applications. The reported concept provides the route for multiple wavefront shaping via a single ultrathin nanoscale photonic device that can integrate with nanoelectronic circuits, ushering in a new era of light manipulation.

■ ASSOCIATED CONTENT

Ⓢ Supporting Information

The Supporting Information is available free of charge on the ACS Publications website at DOI: 10.1021/acsphotonics.5b00113.

■ AUTHOR INFORMATION

Corresponding Author
*E-mail: mehasman@technion.ac.il.
Notes
The authors declare no competing financial interest.

■ ACKNOWLEDGMENTS

■ REFERENCES

(1) Bomzon, Z.; Kleiner, V.; Hasman, E. Computer-generated space-variant polarization elements with subwavelength metal stripes. *Opt. Lett.* **2001**, *26*, 33−35.

(2) Bomzon, Z.; Biener, G.; Kleiner, V.; Hasman, E. Space-variant Pancharatnam-Berry phase optical elements with computer-generated subwavelength gratings. *Opt. Lett.* **2002**, *27*, 1141−1143.

(3) Kildishev, A. V.; Boltasseva, A.; Shalaev, V. M. Planar photonics with metasurfaces. *Science* **2013**, *339*, 1232009.

(4) Yu, N.; Capasso, F. Flat optics with designer metasurfaces. *Nat. Mater.* **2014**, *13*, 139−150.

(5) Yu, N.; Genevet, P.; Kats, M. A.; Aieta, F.; Tetienne, J.-P.; Capasso, F.; Gaburro, Z. Light propagation with phase discontinuities: Generalized laws of reflection and refraction. *Science* **2011**, *334*, 333−337.

(6) Yin, X.; Ye, Z.; Rho, J.; Wang, Y.; Zhang, X. Photonic spin Hall effect at metasurfaces. *Science* **2013**, *339*, 1405−1407.

(7) Lin, D.; Fan, P.; Hasman, E.; Brongersma, M. L. Dielectric gradient metasurface optical elements. *Science* **2014**, *345*, 298−302.

(8) Papakostas, A.; Potts, A.; Bagnall, D. M.; Prosvirnin, S. L.; Coles, H. J.; Zheludev, N. I. Optical manifestations of planar chirality. *Phys. Rev. Lett.* **2003**, *90*, 107404.

(9) Shitrit, N.; Bretner, I.; Gorodetski, Y.; Kleiner, V.; Hasman, E. Optical spin Hall effects in plasmonic chains. *Nano Lett.* **2011**, *11*, 2038−2042.

(10) Huang, L.; Chen, X.; Mühlenbernd, H.; Li, G.; Bai, B.; Tan, Q.; Jin, G.; Zentgraf, T.; Zhang, S. Dispersionless phase discontinuties for controlling light propagation. *Nano Lett.* **2012**, *12*, 5750−5755.

(11) Hasman, E.; Kleiner, V.; Biener, G.; Niv, A. Polarization dependent focusing lens by use of quantized Pancharatnam-Berry phase diffractive optics. *Appl. Phys. Lett.* **2003**, *82*, 328−330.

(12) Ni, X.; Ishii, S.; Kildishev, A. V.; Shalaev, V. M. Ultra-thin, planar, Babinet-inverted plasmonic metalenses. *Light Sci. Appl.* **2013**, *2*, e72.

(13) Sun, S.; He, Q.; Xiao, S.; Xu, Q.; Li, X.; Zhou, L. Gradient-index meta-surfaces as a bridge linking propagating waves and surface waves. *Nat. Mater.* **2012**, *11*, 426−431.

(14) Brongersma, M. L.; Shalaev, V. M. The case for plasmonics. *Science* **2010**, *328*, 440−441.

(15) Sun, J.; Wang, X.; Xu, T.; Kudyshev, Z. A.; Cartwright, A. N.; Litchinitser, N. M. Spinning light on the nanoscale. *Nano Lett.* **2014**, *14*, 2726−2729.

(16) Pors, A.; Albrektsen, O.; Radko, I. P.; Bozhevolnyi, S. I. Gap plasmon-based metasurfaces for total control of reflected light. *Sci. Rep.* **2013**, *3*, 2155.

(17) Berry, M. V. The adiabatic phase and Pancharatnam's phase for polarized light. *J. Mod. Opt.* **1987**, *34*, 1401−1407.

(18) Rodríguez-Fortuño, F. J.; Marino, G.; Ginzburg, P.; O'Connor, D.; Martínez, A.; Wurtz, G. A.; Zayats, A. V. Near-field interference for the unidirectional excitation of electromagnetic guided modes. *Science* **2013**, *340*, 328−330.

(19) Lin, J.; Mueller, J. P. B.; Wang, Q.; Yuan, G.; Antoniou, N.; Yuan, X.-C.; Capasso, F. Polarization-controlled tunable directional coupling of surface plasmon polaritons. *Science* **2013**, *340*, 331−334.

(20) Shitrit, N.; Maayani, S.; Veksler, D.; Kleiner, V.; Hasman, E. Rashba-type plasmonic metasurface. *Opt. Lett.* **2013**, *38*, 4358−4361.

(21) Shitrit, N.; Yulevich, I.; Kleiner, V.; Hasman, E. Spin-controlled plasmonics via optical Rashba effect. *Appl. Phys. Lett.* **2013**, *103*, 211114.

(22) Shalaev, V. M. *Nonlinear Optics of Random Media: Fractal Composites and Metal-Dielectric Films*; Springer: Berlin, 2000.

(23) Wiersma, D. S. Disorded photonics. *Nat. Photonics* **2013**, *7*, 188−196.

(24) Segev, M.; Silberberg, Y.; Christodoulides, D. N. Anderson localization of light. *Nat. Photonics* **2013**, *7*, 197−204.

(25) Wolf, P. E.; Maret, G. Weak localization and coherent backscattering of photons in disordered media. *Phys. Rev. Lett.* **1985**, *55*, 2696−2699.

(26) Pendry, J. B.; MacKinnon, A.; Pretre, A. B. Maximal fluctuations − a new phenomenon in disordered systems. *Phys. (Amsterdam, Neth.)* **1990**, *168A*, 400−407.

(27) Vellekoop, I. M.; Mosk, A. P. Universal optimal transmission of light through disordered materials. *Phys. Rev. Lett.* **2008**, *101*, 120601.

(28) Vellekoop, I. M.; Mosk, A. P. Focusing coherent light through opaque strongly scattering media. *Opt. Lett.* **2007**, *32*, 2309−2311.

(29) Popoff, S. M.; Lerosey, G.; Carminati, R.; Fink, M.; Boccara, A. C.; Gigan, S. Measuring the transmission matrix in optics: An approach to the study and control of light propagation in disordered media. *Phys. Rev. Lett.* **2010**, *104*, 100601.

(30) Vynck, K.; Burresi, M.; Riboli, F.; Wiersma, D. S. Photon management in two-dimensional disordered media. *Nat. Mater.* **2012**, *11*, 1017−1022.

(31) Stockman, M. I. Inhomogeneous eigenmode localization, chaos, and correlations in large disordered clusters. *Phys. Rev. E* **1997**, *56*, 6494−6507.

(32) Savo, S.; Papasimakis, N.; Zheludev, N. I. Localization of electromagnetic fields in disordered metamaterials. *Phys. Rev. B* **2012**, *85*, 121104.

(33) Xu, T.; Jiao, X.; Zhang, G. P.; Blair, S. Second-harmonic emission from sub-wavelength apertures: Effects of aperture symmetry and lattice arrangement. *Opt. Exp.* **2007**, *15*, 13894−13906.

(34) Allen, L.; Beijersbergen, M. W.; Spreeuw, R. J. C.; Woerdman, J. P. Orbital angular momentum of light and the transformation of Laguerre-Gaussian laser modes. *Phys. Rev. A* **1992**, *45*, 8185−8189.

(35) Shitrit, N.; Nechayev, S.; Kleiner, V.; Hasman, E. Spin-dependent plasmonics based on interfering topological defects. *Nano Lett.* **2012**, *12*, 1620−1623.

(36) Robinson, I. K.; Tweet, D. J. Surface X-ray diffraction. *Rep. Prog. Phys.* **1992**, *55*, 599−651.

(37) Caflisch, R. E. Monte Carlo and quasi-Monte Carlo methods. *Acta Numer.* **1998**, *7*, 1−49.

(38) Goodman, J. W. Some fundamental properties of speckle. *J. Opt. Soc. Am.* **1976**, *66*, 1145−1150.

(39) Maniloff, E. S.; Johnson, K. M. Maximized photorefractive holographic storage. *J. Appl. Phys.* **1991**, *70*, 4702−4707.

(40) Miller, D. A. B. Rationale and challenges for optical interconnects to electronic chips. *Proc. IEEE* **2000**, *88*, 728−749.

(41) Gabor, D. In *Progress in Optics*; Wolf, E., Ed.; North-Holland: Amsterdam, 1961; Vol. *1*, pp 109−153.

(42) Davidson, N.; Friesem, A. A.; Hasman, E. On the limits of optical interconnects. *Appl. Opt.* **1992**, *31*, 5426−5430.